ACS OMEGA

Open Access

http://pubs.acs.org/journal/acsodf

Article

In Situ Formation of Hydrogels Loaded with ZnO Nanoparticles Promotes Healing of Diabetic Wounds in Rats

Jun Wang,[§] Cheng-Nan Zhang,[§] Xun Xu,[§] Tian-Ci Sun, Ling-Chao Kong,* and Ren-De Ning*

Cite This: *ACS Omega* 2024, 9, 51442−51452

Read Online

ACCESS | Metrics & More | Article Recommendations

ABSTRACT: The challenge of healing diabetic skin wounds presents a significant hurdle in clinical practice and scientific research. In response to this pressing concern, we have developed a temperature-sensitive, in situ-forming hydrogel comprising poly(*n*-isopropylacrylamide$_{166}$-*co*-*n*-butyl acrylate$_9$) -poly-(ethylene glycol) -poly(*n*-isopropylacrylamide$_{166}$-*co*-butyl acrylate$_9$) copolymer, denoted as PEP, in combination with zinc oxide nanoparticles, forming what we refer to as PEP-ZnO hydrogel. The antimicrobial properties of the PEP-ZnO hydrogel against methicillin-resistant *Staphylococcus aureus* were rigorously assessed by using the bacteriostatic banding method. In vitro evaluations encompassed examinations of hemocompatibility and biocompatibility. The study further employed a diabetic Sprague−Dawley (SD) rat whole-layer trauma model for comprehensive in vivo analyses. In vivo healing assessments revealed the potential of the PEP-ZnO hydrogel, characterized by increased collagen deposition and enhanced vascularization at the trauma site, thus significantly expediting the healing process. Collectively, these findings endorse the PEP-ZnO hydrogel as a safe and effective dressing for addressing chronic wounds in diabetic patients. This hydrogel not only holds promise for improving the quality of life for diabetic individuals grappling with chronic wounds but also represents a noteworthy advancement in wound care.

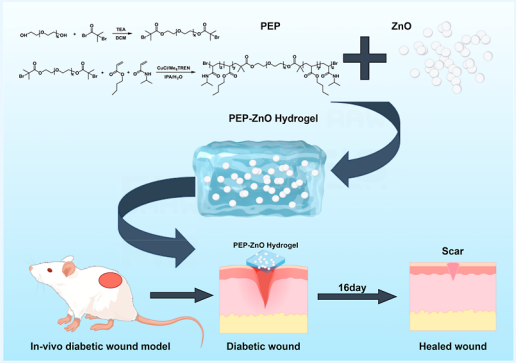

INTRODUCTION

Diabetes mellitus (DM) is a chronic metabolic disorder that frequently leads to skin complications.[1] Nearly 500 million individuals worldwide grapple with diabetes, and this number is expected to surge in the coming years.[2] Vascular damage induced by elevated blood glucose plays a pivotal role in severe diabetic complications.[3] Disturbingly, one-third to one-fifth of people with DM will experience chronic, nonhealing wounds, like diabetic foot ulcers (DFUs), during their lifetime, significantly diminishing the quality of life and imposing a substantial social and economic burden on healthcare systems.[4−7]

Despite debridement, wound dressing, lesion decompression, antimicrobial measures, peripheral vascular disease management, and conventional glycemic control, treatments for DFUs remain insufficient for chronic wounds.[8] Notably, 84% of all lower-limb-amputations caused by diabetes are DFU-related, resulting in significant psychological distress and sometimes death.[9] Consequently, devising superior strategies for managing diabetic chronic wounds has a central objective for both scientific research and clinical practice.[10]

Hemostasis, inflammation, proliferation, and remodeling are the four overlapping phases of the intricate process of healing diabetic chronic wounds.[11,12] Many types of wound dressings have been developed recently to facilitate this process. Conventional wound dressings such as gauze, cotton wool, and polymer bandages are ineffective at maintaining a moist wound environment or preventing bacterial infection.[13] Contrast, hydrogels have become more popular due to their high-water content and three-dimensional (3D) architecture. To accelerate the healing of damaged skin, wound dressings may be enriched with antimicrobials, antioxidants, cytokines, or therapeutic stem cells.[14] Thus, designing biomaterials that effectively regulate cellular biological activities in the wound microenvironment, especially during tissue remodeling, healing, and inflammation, is now essential.[15,16] Such materials can potentially provide an ideal milieu for long-term skin injury healing. In situ forming hydrogels have emerged as a viable material for wound treatment, according to recent developments.[17] An ideal in situ-forming hydrogel wound dressing should possess antibacterial properties against drug-resistant bacteria like methicillin-resistant *Staphylococcus aureus* (MRSA), and rapid in situ gelation with high stability, injectability, and safety.[18,19]

Received: September 19, 2024
Revised: December 1, 2024
Accepted: December 9, 2024
Published: December 17, 2024

Combating infections represents a major clinical challenge in diabetic wound care.[20] Conventional synthetic organic antibiotics often demonstrate limited efficacy against MRSA.[21] Thus, nanoparticles with antimicrobial properties, such as zinc oxide, graphene oxide, and titanium dioxide, have garnered substantial research interest.[22] Zinc oxide (ZnO) nanoparticles are promising candidates for active components in wound dressings due to their antibacterial properties and ability to stimulate angiogenesis and fibroblast proliferation.[23,24] This work presents an irreversible, temperature-sensitive in situ-forming hydrogel to create a multifunctional antibacterial prohealing hydrogel that accelerates the healing of diabetic chronic wounds.

ZnO nanoparticles are incorporated within this hydrogel and are well-known for their antibacterial properties. This irreversible hydrogel forms in situ upon meeting the wound, providing long-term wound dressing efficacy through its unique combination of biosafety, antimicrobial activity against MRSA, and wound-healing stimulation. Based on trials performed on skin wounds, this hydrogel shows promise for accelerating the healing of chronic diabetic lesions.

MATERIALS AND METHODS

Preparation of PEP Copolymers. Briefly, 3.4 g of 2-bromo-2-methylpropionyl bromide (14.8 mmol), 15.0 g of PEG (3.75 mmol, 4 kDa), and 1.8 g of triethylamine (17.8 mmol) were added into 150 mL of dichloromethane and stirred under N_2 at 0 °C. After 72 h, the macroinitiator (Br-PEG-Br) was obtained by dialysis against water followed by freeze-drying.[25] PEP copolymers were synthesized by typical atom transfer radical polymerization as follows: 2.5 g of NIPAM (22.1 mmol), 0.16 g of nBA (1.2 mmol), 28.6 mg of CuCl (0.3 mmol), and 0.21 g of macroinitiator (0.05 mmol) were dissolved in isopropanol/water (95/5 by w/w %). After deoxygenation, the microsyringe added 80.3 mg of Me6TREN (0.36 mmol) to the mixed solution. The polymerization was carried out at room temperature for 72 h. After passing the reaction mixture through an Al_2O_3 column and precipitating in cold *n*-hexane, the final product (conversion 78%), poly(*N*-isopropylacrylamide$_{166}$-*co*-*n*-butyl acrylate$_9$)-poly(ethylene glycol)-poly(*N*-isopropylacrylamide$_{166}$-*co*-*n*-butyl acrylate$_9$), was obtained as a white solid.

Preparation of the Composite Hydrogel. Normal saline (25 wt %) was mixed with PEP copolymer and refrigerated at 4 °C for a full day. ZnO nanoparticles (0.2 wt %) were added to the PEP polymer solution and heated above 25 °C to create a PEP-ZnO hybrid hydrogel.

Hydrogel Characterizations. NMR spectra were recorded on an Agilent VNMRS600 instrument. A Thermo Nicolet 67 instrument was used to perform Fourier transform infrared spectroscopy. The polymers' absolute molecular weights and polydispersities were determined using triple detection (refractive index, multiangle laser-light scattering, and viscosity) gel permeation chromatography (GPC) (Agilent PLGPC 50). Using a Zeiss Supra instrument, scanning electron microscopy (SEM) was conducted. An infrared thermal imaging system, a 40A Fluke Ti400, was employed. A 20 mm parallel plate arrangement on an Anton Paar MCR302 rheometer was used to record the storage/loss modulus (G'/G'').

Zn^{2+} Release. The hydrogel was immersed in a wound simulation solution (5 mL) and incubated in a shaker at 100 rpm at 37 °C. Released Zn^{2+} was quantified at different times by an atomic absorption spectrophotometer (AA-6800, Shimadzu, Japan).

CCK-8 Analysis. The biosafety of PEP-ZnO hydrogels was evaluated by using mouse embryonic cell fibers (NIH-3T3) and human umbilical vein cells (HUVECs). First, 2500 HUVEC or NIH-3T3 cells were seeded into each well of 96-well plates. The cells were then incubated for 24 h at 37 °C with 5% CO_2. When the incubation period was over, the medium was carefully removed and replaced with fresh medium. The prepared PEP-ZnO hydrogel was added to the wells, while the blank control wells received the same grade of PBS buffer. The incubation was continued for 24 h; the old medium was removed, and each well was carefully washed three times with PBS buffer to remove any residual medium. Next, 100 μL of medium and 10 μL of CCK-8 reagent were added to each well using a pipet gun. The plate was then incubated for another 2 h at 37 °C and 5% CO_2. Finally, the absorbance (OD) of each well was determined at 450 nm wavelength by using a spectrometer.

Cell viability was calculated using the following formula:

$$\text{cell viability} = \frac{\text{OD}'}{\text{OD}''} \times 100\%$$

where OD′ represents the PEP-ZnO hydrogel absorbance and OD″ represents the absorbance of the blank control group.

Hemolytic Analysis. In this study, we utilized rat whole blood cells to evaluate the hemocompatibility of hydrogel.[26] Specifically, 2 mL of fresh SD rat whole blood was extracted and centrifuged at 1300 rpm for 15 min. Specifically, 2 mL of fresh SD rat whole blood was withdrawn and centrifuged at 1300 rpm for 15 min to obtain the RBCs that precipitated into the lower layer. This process was repeated 2−3 times with PBS. The pure RBCs were then diluted to 5% with PBS. The sample was divided into three distinct groups. In each group, 100 μL of PEP-ZnO hydrogel sample solution, 100 μL of 0.9% NaCl solution, and 100 μL of DI water were added along with 500 μL of the erythrocyte dilution into 2 mL centrifugal tubes. These served as the experimental group, negative control, and positive control, respectively. Using a pipet, the sample was gently mixed and then incubated at 37 °C for 1 h, the samples were centrifuged at 1300 rpm for 10 min. The supernatant was carefully aspirated into the centrifuge tube and centrifuged again for 10 min. The supernatant was carefully aspirated into a 96-well plate, and the OD was measured at 540 nm. The hemolysis ratio was calculated as follows:

$$\text{hemolysis ratio} = \frac{A' - A''}{A''' - A''} \times 100\%$$

where A' represents the OD value of the sample and A'' and A''' represent the OD values of the positive and negative control groups, respectively.

Biochemical and Degradability Analysis. 10 SD rats (male, 200 ± 25 g) were randomly divided into two groups and injected subcutaneously with saline and PEP-ZnO hydrogel, respectively. The rats were executed by the cervical vertebral dissection method after 10 days, and blood was collected for liver and kidney function analysis. The in vitro degradation characteristics of PEP-ZnO hydrogels were determined by placing them in sterile 1× PBS for up to 6 weeks. Before the experiment, the PEP-ZnO hydrogel was weighed (m_0), sterilized under UV light, and placed in a centrifuge tube with an appropriate amount of sterile PBS. The tube was then placed in a constant temperature shaking

https://doi.org/10.1021/acsomega.4c08537
ACS Omega 2024, 9, 51442−51452

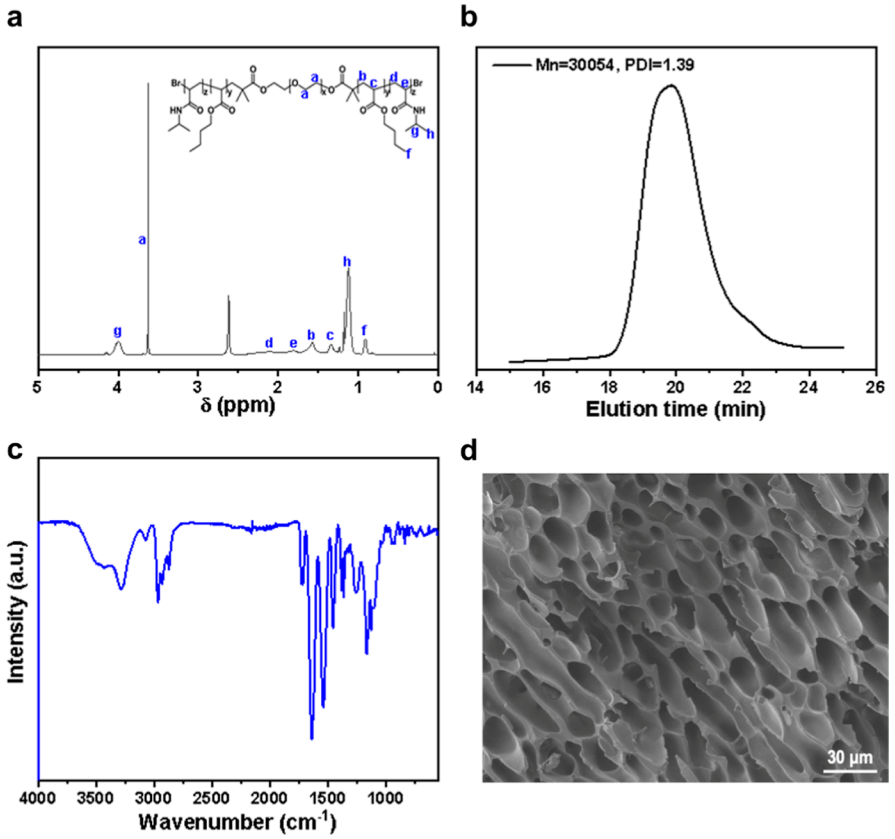

Figure 1. Characterization of PEP hydrogel: (a) ^{1}H NMR spectra of PEP. (b) GPC spectra of PEP. (c) FTIR spectra of PEP. (d) SEM image of porous structures in PEP hydrogel.

chamber at 37 °C (n = 3). The hydrogel was removed at the present points, rinsed with DI-Water, and dried in a vacuum drying oven. Once the sample reached a stable quality, it was weighed (m_t). The residual mass percentage of the PEP-ZnO hydrogel was calculated using the following formula:

$$\text{residual mass percentage} = \frac{m_t}{m_0} \times 100\%$$

Antimicrobial Activity. MRSA (Mu50) was used to evaluate the antibacterial effect of the PEP-ZnO hydrogel. 100 μL of a diluted bacterial suspension (106 CFU/mL) was uniformly applied on LB agar plates. Then, an appropriate amount of PEP-ZnO hydrogel samples was placed on agar plates of MRSA. The antibacterial effect of these samples was evaluated by measuring the diameter of the inhibition zone after incubation at 37 °C for 24 h and 48 h, and the experiments were carried out in three groups with the average values taken.[27] The in vivo antimicrobial test was carried out on SD rats anesthetized by intraperitoneal injection of chloral hydrate (10%, 0.3 mL per 100 g of body weight). Their backs were shaved, and two full-thickness circular skin wounds (approximately 0.8 cm diameter) were created on either side of the dehaired area on the dorsal surface. To establish an MRSA-infected wound model, MRSA suspension (100 μL, 10^6 CFU/mL) was inoculated into the wound. Bacterial samples were collected from the wound surface with sterilized swabs at 2 h postinfection (before hydrogel dressing) and 10 days post-treatment. The collected swabs were placed in 0.5 mL of saline, and the surviving MRSA load in the diluted bacterial suspension was preliminarily investigated on LB agar plates at 37 °C.

Diabetic Rat Model. SD rats (male, 200 ± 25 g) were provided by the SPF Animal Experiment Center of University of Science and Technology of China. All rats were maintained in a room with constant temperature (25 °C) and stable humidity with a 12 h light/dark cycle. Streptozotocin (STZ, 50 mg/kg, Sigma, USA) was dissolved in citric acid-sodium citrate buffer (pH 4.4) to obtain a 1% STZ solution and then intraperitoneally injected into SD rats after an 18 h fast to induce diabetes. Rats with blood glucose over 16.67 mmol/L one-week postinjection were diagnosed as diabetic. The wound healing model was established 3 weeks after diabetes onset post-STZ. Rats were imported, transported, housed, and bred recommendations for the research on nonhuman primates. Rats were euthanized via cervical dislocation to prevent suffering. The Animal Care and Use Committee of Anhui Medical University approved all procedures involving animals.

Surgical Procedure. 36 diabetic rats were anesthetized with pentobarbital (35 mg/kg, Sigma, USA) by intraperitoneal injection 3 weeks after STZ-induced hyperglycemia. Following anesthesia, the dorsal skin was scraped and disinfected with 75% ethanol. Two symmetrical full-thickness skin wounds of 8 mm diameter were created. Rats were randomly divided into three groups for each wound: (a) PBS group; (b) PEP hydrogel group; and (c) PEP-ZnO hydrogel group. Wounds were covered with different materials before being patched with sterile dressings and replaced every 4 days. The rats were housed individually postsurgery. All animal experimental protocols were approved by the Animal Care and Use Committee (IACUC) of Anhui Medical University (LLSC20221240).

https://doi.org/10.1021/acsomega.4c08537
ACS Omega 2024, 9, 51442−51452

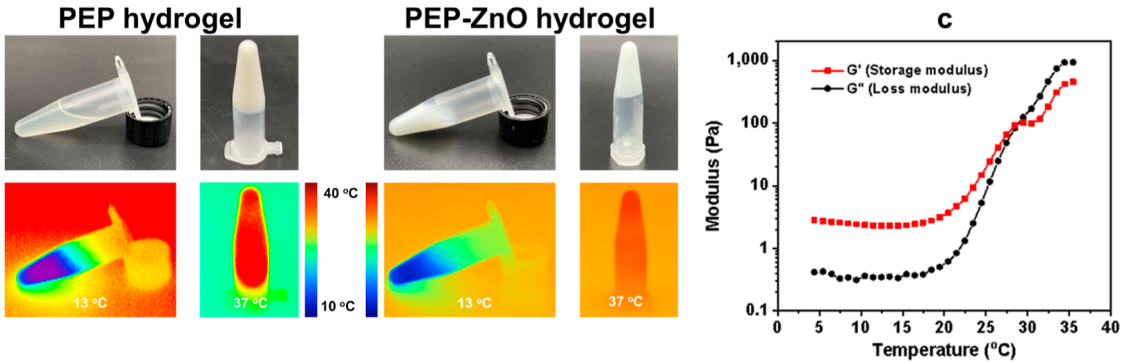

Figure 2. Characterization of PEP-ZnO hydrogel: (a,b) images of PEP and PEP-ZnO aqueous solution taken digitally and infrared thermal imaging during the heating and cooling process. (c) G'/G'' measurements of the PEP and the PEP-ZnO aqueous solution.

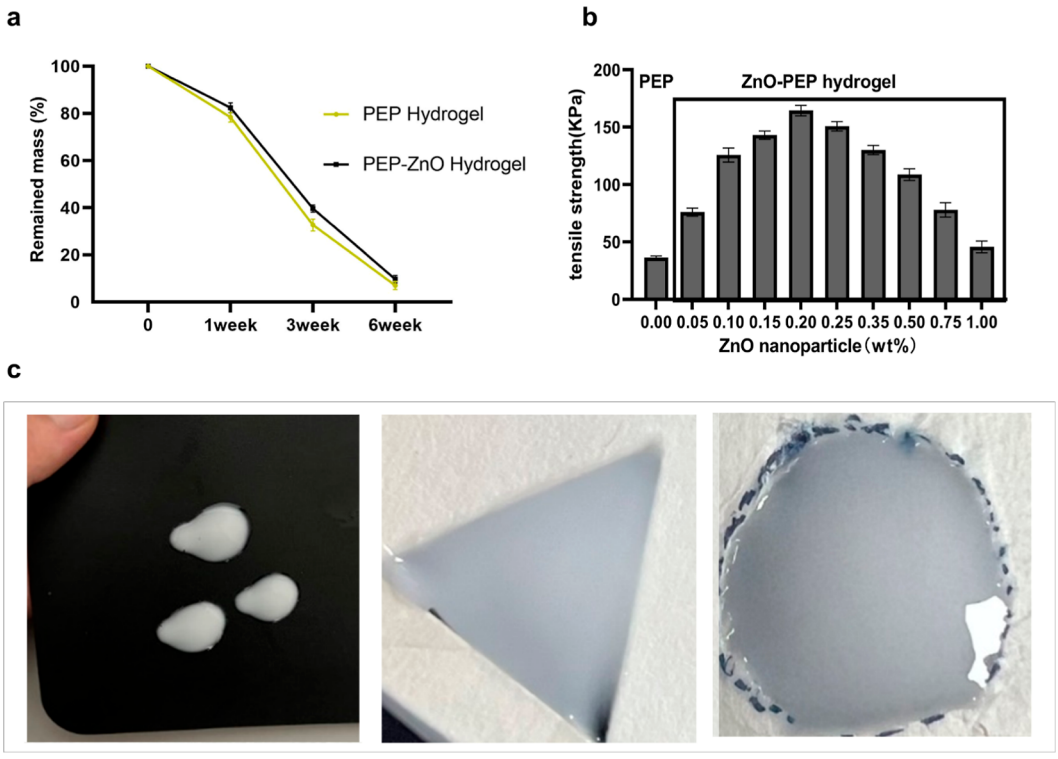

Figure 3. Biocompatibility of PEP-ZnO hydrogels: (a) in vitro degradation rate of PEP-ZnO hydrogel. (b) Tensile strength of PEP-ZnO hydrogels at different ZnO contents. (C) Adhesion and adaptability of PEP-ZnO hydrogels.

Analysis of Wound Closure Rate. Survival and wound healing were observed in each group. Changes in the size of individual diabetic wounds were determined from photographs taken on postoperative days 0, 4, 8, and 16 and analyzed by ImageJ (NIH, USA). The wound areas were calculated and used to obtain the wound healing rate (WHR) by the following equation:

$$\mathrm{WHR} = \frac{S_0 - S_A}{S_0} \times 100\%$$

where S_0 is the area of the wound on day 0 and S_A is the area of the wound on day A.

H&E Staining. The experimental and control rats were euthanized at the specified time point, and wound tissue was collected for histological analysis to evaluate the effects of PEP-ZnO hydrogel on wound healing. Tissue samples were fixed in 10% formalin solution, dehydrated in graded alcohol, and embedded in paraffin wax. Suitable thickness of slices was cut using a microtome, stained with hematoxylin and eosin (H&E), and examined under a light microscope.

Histopathological Assay. For immunohistochemical (IHC) evaluation, skin wound tissue was also excised on postoperative days 8 and 16. Immunohistochemistry was used to detect IL-6, CD31, Collagen-1, and TGF-β to evaluate the effect of the PEP-ZnO hydrogel on wound healing.

Statistical Analysis. Means, standard deviations, and p-values were calculated in GraphPad Prism 9.0 and ImageJ. Experimental data were analyzed using unpaired Student's t-test. $^{*}p \leq 0.05$ and $^{**}p \leq 0.01$. All results are expressed as the mean. All error bars represent the standard deviation.

RESULTS AND DISCUSSION

In Situ Formation of PEP-ZnO Hydrogels. We employed a biocompatible block copolymer, P(NIPAM$_{166}$-*co*-nBA$_9$)-PEG-P(NIPAM$_{166}$-*co*-nBA$_9$), with a molecular weight,

https://doi.org/10.1021/acsomega.4c08537
ACS Omega 2024, 9, 51442−51452

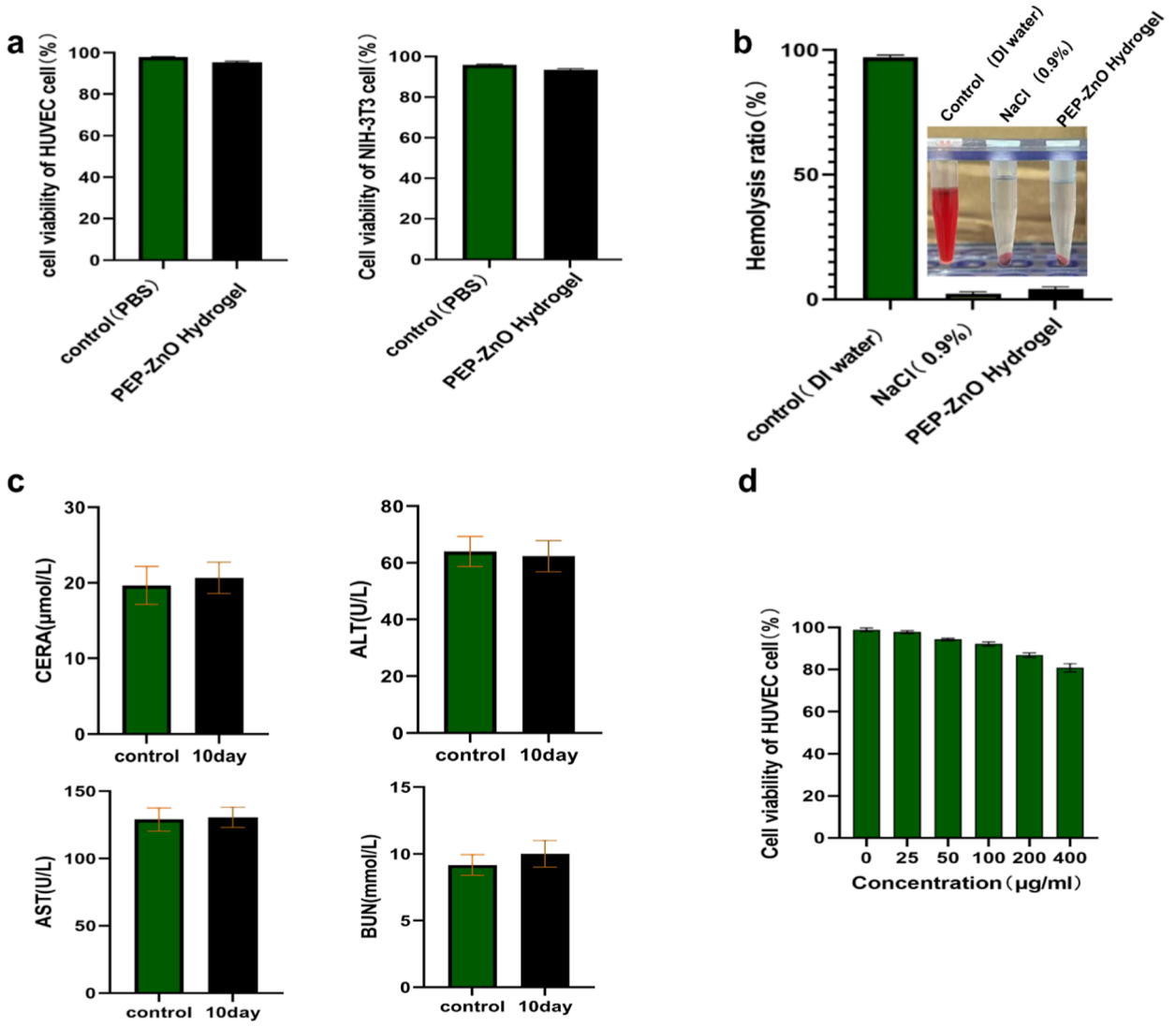

Figure 4. Biocompatibility of PEP-ZnO hydrogels: (a) biocompatibility of PEP-ZnO hydrogel on HUVEC cells and NIH-3T3 cells. (b) Blood compatibility of PEP-ZnO hydrogel (n = 5). (c) Evaluation of liver and kidney function of rats 10 days after the administration of the PEP-ZnO hydrogel (n = 5). (d) Cell viability tests of varying ZnO concentrations.

to fabricate the thermoresponsive polymeric matrix known as PEP (Mn, GPC: 30,054, PDI: 1.39), which was utilized in subsequent experiments (Figure 1b). The ^{1}H NMR spectra and FTIR are shown in Figure 1a,c. A scanning electron microscope view of the typical porous structure of the PEP is shown in Figure 1d. From these SEM images, the average pore sizes of PEP were 8.02 ± 3.15 μm. To provide antimicrobial activity to the PEP hydrogel, ZnO nanoparticles were homogeneously dispersed into the aqueous solution of the PEP polymer. It was tested whether the addition of ZnO would affect the temperature responsiveness of the PEP polymer. As shown in Figure 2a,b, PEP and PEP-ZnO hydrogel transitions from a liquid state at a low temperature (13 °C) to a gel state at a high temperature (37 °C). Rheological tests showed that the hydrogels' storage and loss modulus also showed significant phase aggregation and separation as the temperature changed. The storage and loss modulus (G' and G'') data curves overlap around 28 °C, indicating a low critical solvation temperature (LCST) of around 28 °C. PEP-ZnO copolymers exhibit a typical thermosensitive sol−gel transition (Figure 2c). When the temperature was increased, the PNIPAM chains of the hydrogel were broken, and hydrophobic substances were formed. This may be because the hydrogen bond between PNIPAM and water breaks with increasing temperature. At the same time, the polyethylene glycol chains act as a bridge to cross-link neighboring hydrophobic substances. However, it presents an aqueous state at low temperatures because PNIPAM is hydrophilic at low temperatures (<LCST), while the aggregation of hydrophobic substances may disintegrate. It demonstrates superior temperature responsiveness. This is significant as the human body temperature is around 37 °C, which is substantially higher than the LCST. Wound dressings made of hydrogels should possess excellent mechanical qualities to meet the needs of human soft tissue.[28] We examined the mechanical properties of several PEP-ZnO hydrogels with different concentrations of ZnO nanoparticles. The tensile strength of the composite hydrogel increases gradually as the ZnO nanoparticle content rises from 0% to 0.2 wt %, as shown in Figure 3b. The PEP-ZnO (0.2 wt %) hydrogel has a tensile stress of 164 kPa, which is 4.5 times greater than the hydrogel made solely of PEP (36.4 kPa). However, the hydrogel's tensile strength abruptly

https://doi.org/10.1021/acsomega.4c08537
ACS Omega 2024, 9, 51442−51452

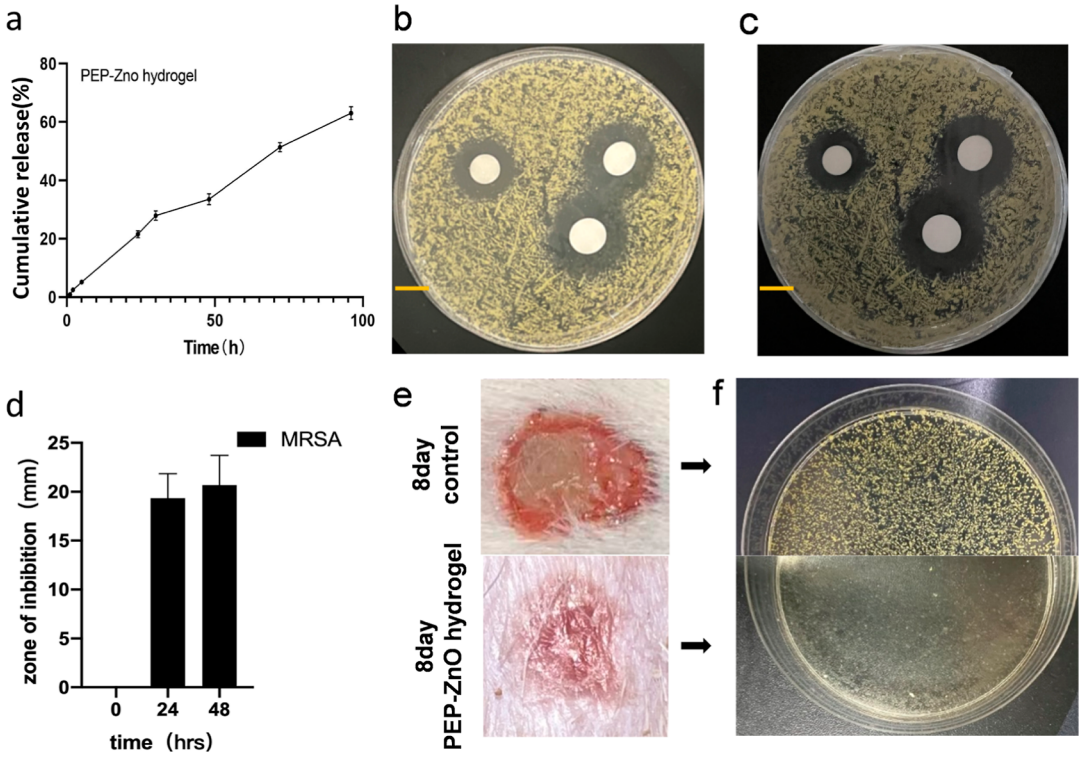

Figure 5. In vivo and in vitro antimicrobial effect of PEP-ZnO hydrogel: (a) controlled release of ZnO in PEP-ZnO hydrogel. (b) MRSA growth image of PEP-ZnO hydrogel group after 24 h. (c) MRSA growth image of PEP-ZnO hydrogel group after 48 h. (d) Diameter of the inhibition zone of PEP-ZnO hydrogel. (e) Photographs of MRSA-infected wounds in rats at day 8 (n = 5). (f) Bacterial culture of MRSA-infected wound secretions on day 8. Scale bar:10 mm.

reduced when the ZnO level reached 1 wt %. The phenomenon occurs because ZnO nanoparticles are small and have a large specific surface area. This results in a significant contact area between ZnO and PEP, leading to tight coupling between the two materials. Compared to the PEP monomer, ZnO is uniformly dispersed within the PEP. When external forces are applied, ZnO can absorb energy, passivate the cracks, and impede their expansion, thereby resisting tensile forces. However, as the concentration of the ZnO nanoparticles increases, agglomeration can occur. This clustering of nanoparticles generates more defects, which ultimately reduces the tensile strength of the material.[29] Good adhesion and adaptability are essential for a wound dressing, and Figure 3c shows that the PEP-ZnO hydrogel has both of these qualities. The above results indicate that the PEP-ZnO hydrogel has good potential as a wound dressing.

In Vitro and In Vivo Biocompatible Evaluation. In the use of medical dressings, the degradation rate of the dressing plays a role in influencing the release of the drug loaded into the material to a certain extent. As shown in Figure 3a, the degradation rate of the hydrogel loaded with ZnO remained almost unchanged, and about 9% of the original mass was retained after the sixth week, and the degradation rate of the two materials remained stable during the degradation process, with or without the addition of ZnO.

Although ZnO incorporation imparts antimicrobial properties to PEP, the zinc oxide concentration for wound healing therapy must be optimized as high doses can be toxic to neurons or epithelial cells.[30−32] In Figure 4d, HUVEC cell viability started to decrease at zinc oxide nanoparticle concentrations higher than 100 μg/mL and gradually decreased with increasing concentration. At 400 μg/mL, the cell viability was only 80%.

The CCK-8 assay was utilized to assess the cytotoxicity of the PEP-ZnO hydrogel. Mouse embryonic fibroblasts (NIH-3T3) and HUVECs were employed. Figure 4a shows that the cell survival rates in the PEP-ZnO hydrogel group were (96.65 ± 0.16) and (95.54 ± 0.31), respectively.

Hemolysis is the release of hemoglobin into plasma due to erythrocyte damage, and the hemolysis rate is directly related to the blood compatibility of the biomaterials. As shown in Figure 4b, the hydrogel group showed a light-yellow color; like the negative control PBS group, while the positive control group showed a red color. According to the hemolysis rate analysis, the hemolysis rate of PEP-ZnO hydrogel was less than 5%, indicating good blood compatibility and potential for clinical use. To further investigate the long-term biocompatibility of the PEP-ZnO hydrogel, serum biochemical tests were performed on rats 10 days after subcutaneous injection. The main indexes of liver and kidney functions were within the normal range, suggesting that the composite hydrogel did not cause any severe damage (Figure 4c).

Antimicrobial Study. The developed nano biomaterials should maintain their potential to protect microbial species when used for wound repair and tissue formation. Trace amounts of Zn promote tissue neovascularization, tissue healing, and recovery.[33−35] Additionally, the antibacterial activity of ZnO expands its applications in the biological field. The PEP hydrogel is a kind of porous structure, and the internal porous structure gradually expands or collapses with the slow degradation of the material; at the same time, the ZnO loaded in the PEP hydrogel is also released with the degradation of the material, which is the effect of the release of

https://doi.org/10.1021/acsomega.4c08537
ACS Omega 2024, 9, 51442−51452

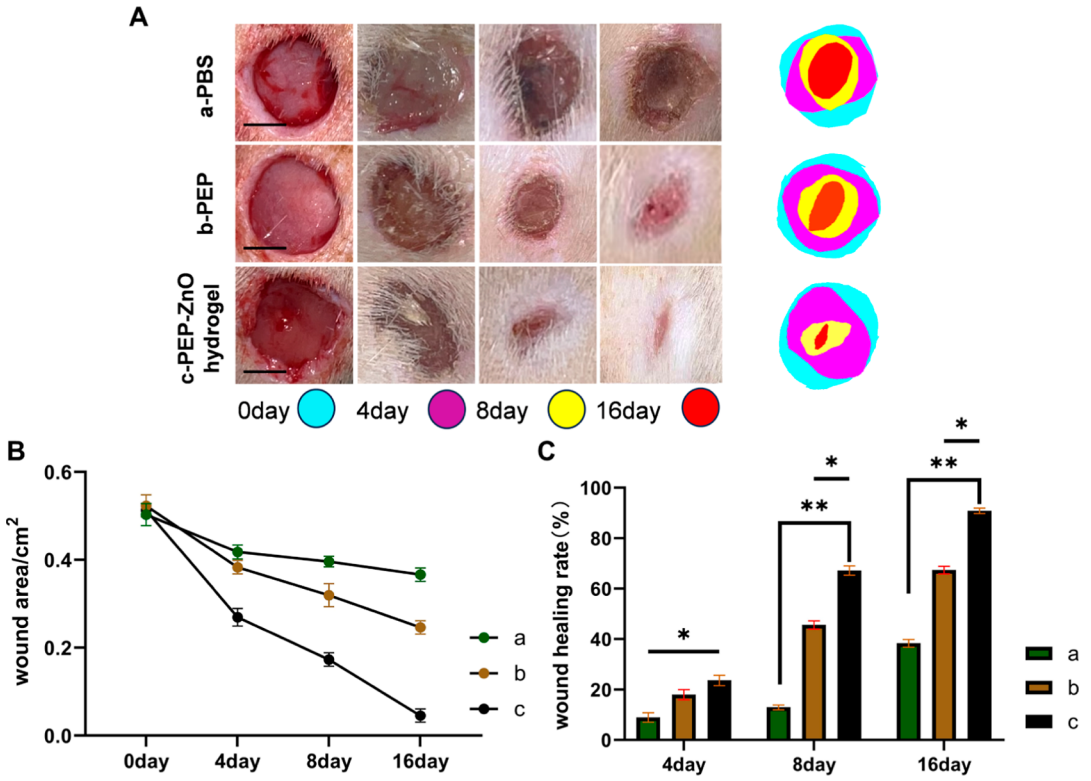

Figure 6. PEP-ZnO hydrogel promoted wound healing in diabetic rats: (A) photographs taken on days 0, 4, 8, and 16 and wound healing superimpositions (error bars are standard deviation, $n = 5$). (B) Wound area of each group. (C) Wound healing rate of each group. (**$P < 0.5$, **$P < 0.01$).

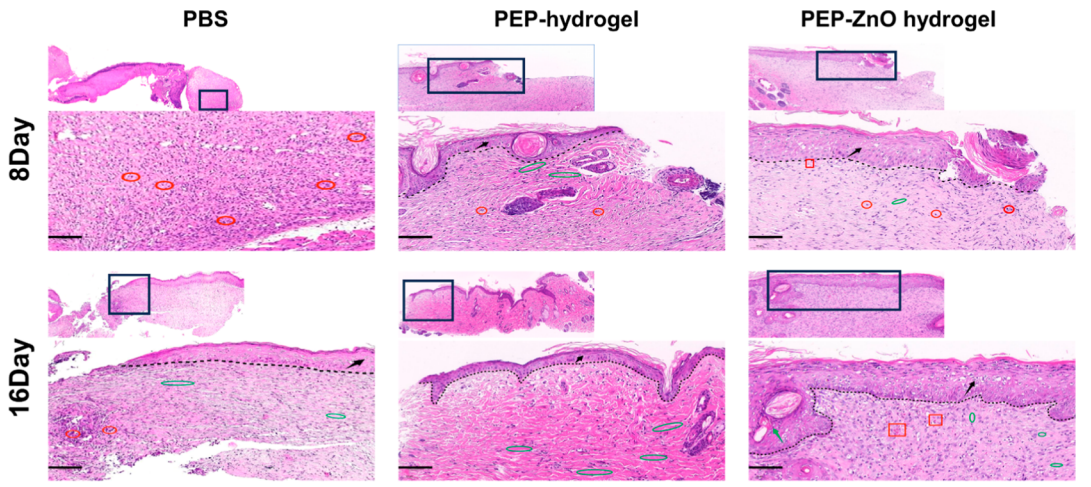

Figure 7. PEP-ZnO hydrogel promoted wound healing in diabetic rats: (A) H&E staining of wounds at day 8 and day 16. Red circles, green circles, red squares, black lines, black arrows, and green arrows represent inflammatory cells, collagen fibers, blood vessels, epidermal−dermal demarcation, epidermis, and skin appendages. Scale bar:100 μm.

drugs loaded in the material. ZnO in the PEP hydrogel was also released with the degradation of the material, which was a slow-release mode of degradation of the outer polymer layer and drug release from the outer surface, followed by a slow-release mode due to the diffusion of the drug from the inner core layer. Benefiting to the porous structure of the PEP hydrogel, as shown in Figure 5a after 96 h, the release rate of ZnO reached 60%, which could control the inflammation of the wound more rapidly and achieve the promotion of the wound healing effect. The sustained release of ZnO nanoparticles gives the hydrogel an antimicrobial long-term impact.

For wound healing, antimicrobials are a priority, especially in chronic wounds, which heal slowly and increase the chances of infection. It has been shown that free zinc ions released from ZnO can accumulate on the surface of cell membranes to form strong ionic bonds, triggering bacterial death, and it has also been shown that ZnO can induce oxidative stress generated by ROS, leading to cell death.[36] As shown in Figure 5, the PEP-ZnO hydrogel exhibits a superior antimicrobial potential. PEP-ZnO hydrogel inhibits MRSA in a zone that measures about 19 mm after 24 h (Figure 5b) and 20 mm after 48 h (Figure 5c). Figure 5e,f demonstrates the strong in vivo antibacterial power

https://doi.org/10.1021/acsomega.4c08537
ACS Omega 2024, 9, 51442−51452

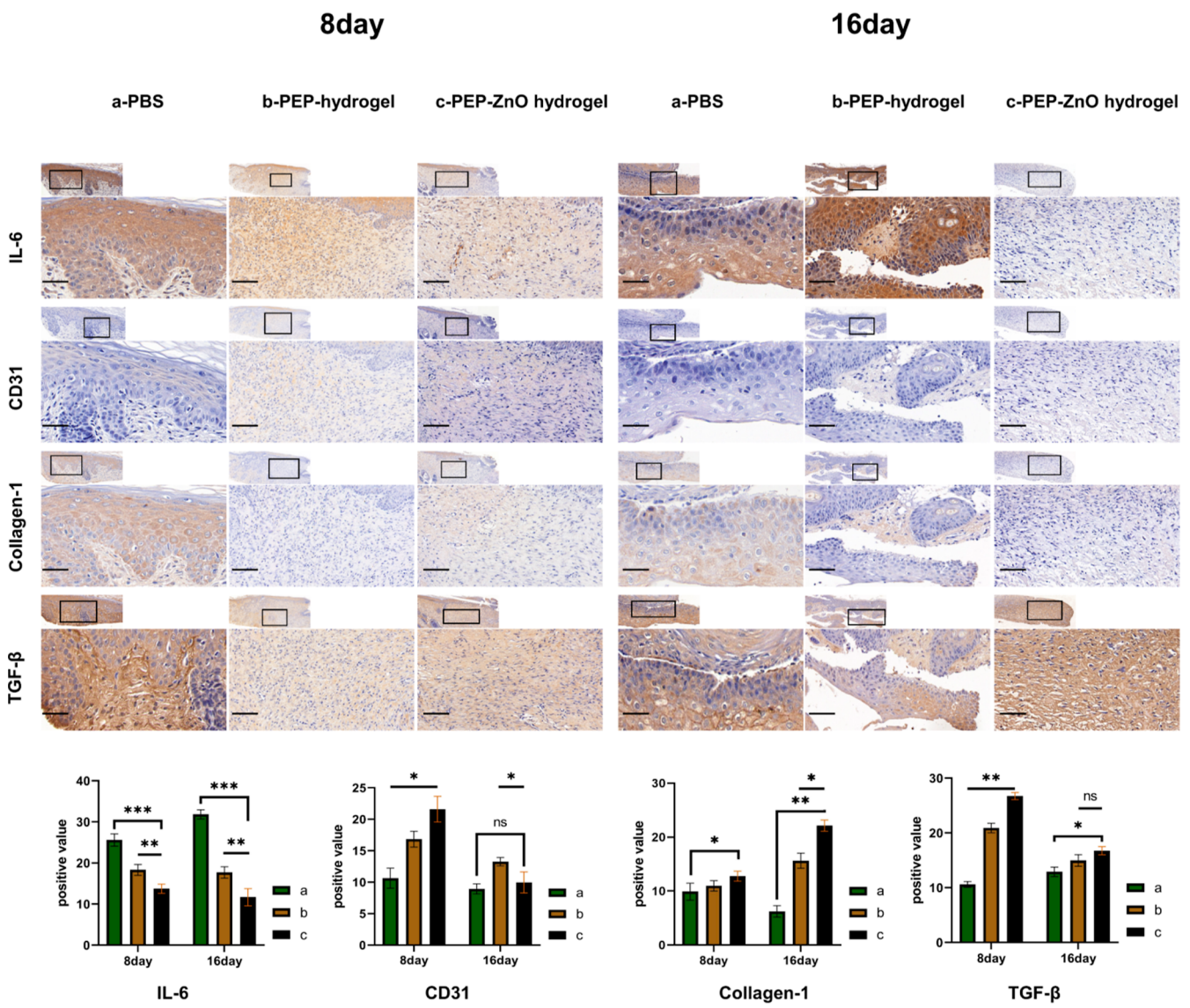

Figure 8. PEP-ZnO hydrogel promoted wound healing in diabetic rats. IHC analysis of skin tissue at the wound site on days 8 and 16 in the PBS, PEP, and PEP-ZnO groups. Scale bar:100 μm. *P < 0.05, **P < 0.01.

of PEP-ZnO hydrogel. The results of the wound secretion culture on the eighth day showed that the PEP-ZnO hydrogel had a good antimicrobial effect.

In Vivo Wound Healing Activity. Diabetic wounds, like nonhealing wounds, have a complex microenvironment and require special medical management.[37] To evaluate the effect of PEP-ZnO hydrogel more intuitively in boosting the healing of entire skin damage in diabetic rats, Figure 6A displays representative wound healing photos of each group at 0, 4, and 16 days postoperatively together with the wound overlaid effect graphs. The area and healing rate of diabetic wounds at days 0, 4, and 16 are displayed in Figure 6B,C, respectively. On postoperative day 4, no significant differences were observed between the PEP hydrogel and PBS groups. At day 16, wounds in the PEP-ZnO hydrogel group were almost completely healed, with wound healing rates in the PEP hydrogel and PBS groups being about 70% and 29%, respectively. The results showed that PEP-ZnO hydrogel could promote the healing of chronic wounds. The process of wound healing involves tissue growth and regeneration, which includes hemostasis, inflammation, proliferation, and remodeling.

Histological Analysis. H&E staining was performed to assess histologic changes during wound healing. Wound healing is a complex process involving inflammatory cells, which produce a variety of substances such as cytokines and transmitters that play an essential role in wound healing. As illustrated in Figure 7, on day 8, a considerable number of inflammatory cells were observed in the control group. In contrast, the PEP-ZnO hydrogel and PEP groups exhibited a paucity of inflammatory cells and a modest number of collagen fibers, accompanied by the emergence of a rudimentary epithelial structure. However, the dermis was more compact in the PEP-ZnO hydrogel group. By day 16, inflammatory cells were still present in the PBS group. In contrast, the PEP-ZnO hydrogel group showed a significant decrease in inflammatory cells and an increase in collagen fibers, which were transformed into a 3D network structure. Notably, appendages such as hair follicles and a small number of blood vessels also appeared. Lower levels of IL-6 indicate a less severe infection, while optimal levels stimulate the inflammatory response and promote the production of growth factors, thereby promoting wound healing. In contrast, high levels of IL-6 may hinder

https://doi.org/10.1021/acsomega.4c08537
ACS Omega 2024, 9, 51442−51452

wound healing.[38−40] As shown in Figure 8A, we examined the results of interleukin-6 (IL-6) immunostaining to assess the degree of inflammation in each group after different treatments. At 8 and 16 days, IL-6 expression in PEP-ZnO hydrogel-treated wounds was significantly less than that in the control group. The positive values on day 16 were 33.45 ± 2.37, 15.84 ± 2.18, and 12.86 ± 2.74. This phenomenon exhibits a comparable pattern to that observed in the H&E results. This may be due to the enhanced anti-inflammatory and antibacterial effects of ZnO. Angiogenesis is essential for wound healing, CD31 is expressed in the endothelial cells of the interstitial compartment of blood vessels and plays a crucial role in the process of angiogenesis, the newly formed vascular system delivers oxygen and nutrients to the wound site and promotes the growth of granulation tissue throughout the process of wound healing vascularization, and the reduction of generation is a sign of nonhealing of DFUs.[41−43] According to the results shown in Figure 8B, the positive values on day 16 were 9.78 ± 2.16, 16.63 ± 2.03, and 20.37 ± 2.75. At day 16, there was no statistically significant difference between the PBS group and PEP-ZnO hydrogel group, probably because of the complexity of the diabetic wound healing process, the difficulty of recovery, and the continued vascular damage caused by the hyperglycemic environment, which does not have a significant pro-angiogenic capacity in the later stages. Similarly, the expression of TGF-β was significantly higher in the PEP-ZnO hydrogel group on the 16th day after treatment, suggesting that PEP-ZnO hydrogel can promote skin healing and reorganization and that these growth factors can promote the synthesis of fibrinogen and regeneration of skin accessory organs. Therefore, the expression of collagen-1 was significantly higher in the PEP-ZnO hydrogel group than that in the PBS group (Figure 8C,D). The elevation of TGF-β may be due to the role of M2 macrophages, which produce growth factors (e.g., TGF-β and VEGF) that stimulate vascular cells, the activation of fibroblasts, the formation of collagen, and a crucial role in the remodeling of the extracellular matrix, which is essential for wound closure.[44,45] The above results show that the PEP-ZnO hydrogel demonstrated remarkable efficacy in the treatment of diabetic wounds in animal models. The hydrogel's ability to consistently deliver ZnO at the wound site, through the removal of wound exudate, exerted an antimicrobial effect, controlled biofilm formation, and facilitated tissue remodeling, collectively contributing to the observed beneficial outcomes.[46]

CONCLUSIONS

Based on our discoveries, we have concluded that the PEP-ZnO hydrogel shows tremendous promise as a valuable wound covering material, especially for the treatment of chronic diabetic wounds, which present a significant challenge globally. While this study has demonstrated the material's impressive healing potential, the precise mechanisms underlying its accelerated wound healing properties must be summarized. We have successfully developed a temperature-sensitive hydrogel that forms in the body by combining PEP with ZnO. The aqueous PEP and ZnO can immediately transition into the hydrogel when the temperature increases by about 28 °C. Skin temperature is higher than this response temperature, Thus, this PEP- ZnO composite hydrogel can be used as an in situ forming wound dressing for skin temperature response. The healing process of diabetic wounds usually shows delayed and incomplete healing processes, which in turn exposes patients to a high risk of infection.[47] PEP-ZnO hydrogel, when used as a diabetic wound dressing, has an excellent slow-release effect on the loaded zinc oxide, which creates a long-lasting aseptic environment for wounds, which is beneficial to the healing of diabetic wounds; second, PEP-ZnO hydrogel has excellent mechanical properties and temperature responsiveness, which can easily cope with irregular diabetic wounds in the state of aqueous solution and reach the deeper layers of the wound directly. ZnO hydrogel has excellent mechanical properties and temperature responsiveness, which can easily cope with irregular diabetic wounds in the aqueous state, reach the deeper layers of the wound, and rapidly gel and adhere to the wound surface under the effect of temperature; in vivo studies have also found that ZnO has anti-inflammatory, vasculature-enhancing, collagen-enhancing, and transforming growth factor-producing effects in the process of wound healing. In addition, cytotoxicity, biochemical, and in vitro degradation experiments confirmed the biocompatibility of the PEP-ZnO hydrogel. The development of the PEP-ZnO hydrogel signifies a significant advancement in improving the lives of diabetic patients grappling with chronic wounds. This innovative covering material not only has the potential to alleviate suffering but also opens new avenues for advancing wound care practices in both the clinical and scientific fields. The histological examinations provide firm evidence supporting the biocompatibility and biosafety of the PEP-ZnO hydrogel. The potential impact of this discovery on addressing chronic diabetic wounds globally cannot be overstated. However, there remains a crucial need to delve deeper into unraveling the precise mechanisms responsible for its accelerated wound healing properties, thereby enriching our understanding of future treatment enhancements. This promising advancement holds significant promise in elevating the standard of wound care practices across clinical and scientific domains.

AUTHOR INFORMATION

Corresponding Authors

Ren-De Ning − *The Third Affiliated Hospital of Anhui Medical University, The First People's Hospital of Hefei, Anhui, Hefei 230000, China*; orcid.org/0000-0002-5355-263X; Email: nrd1972@outlook.com

Ling-Chao Kong − *The Third Affiliated Hospital of Anhui Medical University, The First People's Hospital of Hefei, Anhui, Hefei 230000, China*; Email: konglingchaocn@163.com

Authors

Jun Wang − *The Third Affiliated Hospital of Anhui Medical University, The First People's Hospital of Hefei, Anhui, Hefei 230000, China*

Cheng-Nan Zhang − *The Third Affiliated Hospital of Anhui Medical University, The First People's Hospital of Hefei, Anhui, Hefei 230000, China*

Xun Xu − *The Third Affiliated Hospital of Anhui Medical University, The First People's Hospital of Hefei, Anhui, Hefei 230000, China*

Tian-Ci Sun − *Hefei University of Technology, Anhui, Hefei 230000, China*

Complete contact information is available at: https://pubs.acs.org/10.1021/acsomega.4c08537

Author Contributions

[§]J.W, C.-N.Z., and X.X. contributed equally to this work.

https://doi.org/10.1021/acsomega.4c08537
ACS Omega 2024, 9, 51442−51452

Notes

The authors declare no competing financial interest.

■ ACKNOWLEDGMENTS

This work was financially supported by the research and development projects of the Medical and Health Institution of He Fei (2021YL006).

■ REFERENCES

(1) Zhao, X.; Chang, L.; Hu, Y.; Xu, S.; Liang, Z.; Ren, X.; et al. Preparation of photocatalytic and antibacterial MOF nanozyme used for infected diabetic wound healing. *ACS Appl. Mater. Interfaces* **2022**, *14* (16), 18194−18208.
(2) Cho, N. H.; Shaw, J. E.; Karuranga, S.; Huang, Y.; da Rocha Fernandes, J. D.; Ohlrogge, A. W.; Malanda, B. IDF Diabetes Atlas: Global estimates of diabetes prevalence for 2017 and projections for 2045. *Diabetes Res. Clin. Pract.* **2018**, *138*, 271−281.
(3) Spampinato, S. F.; Caruso, G. I.; De Pasquale, R.; Sortino, M. A.; Merlo, S. The treatment of impaired wound healing in diabetes: looking among old drugs. *Pharm.* **2020**, *13* (4), 60.
(4) Khan, M. A. B.; Hashim, M. J.; King, J. K.; Govender, R. D.; Mustafa, H.; Al Kaabi, J. Epidemiology of type 2 diabetes−global burden of disease and forecasted trends. *J. Epidemiol. Global Health* **2020**, *10* (1), 107.
(5) Xiao, J.; Zhu, Y.; Huddleston, S.; Li, P.; Xiao, B.; Farha, O. K.; Ameer, G. A. Copper Metal-Organic Framework Nanoparticles Stabilized with Folic Acid Improve Wound Healing in Diabetes. *ACS Nano* **2018**, *12* (2), 1023−1032.
(6) Davis, F. M.; Kimball, A.; Boniakowski, A.; Gallagher, K. Dysfunctional Wound Healing in Diabetic Foot Ulcers: New Crossroads. *Curr. Diabetes Rep.* **2018**, *18* (1), 2.
(7) Brumberg, V.; Astrelina, T.; Malivanova, T.; Samoilov, A. Modern wound dressings: hydrogel dressings. *Biomedicines* **2021**, *9* (9), 1235.
(8) Vijayakumar, V.; Samal, S. K.; Mohanty, S.; Nayak, S. K. Recent advancements in biopolymer and metal nanoparticle-based materials in diabetic wound healing management. *Int. J. Biol. Macromol.* **2019**, *122*, 137−148.
(9) Brem, H.; Tomic-Canic, M. Cellular and molecular basis of wound healing in diabetes. *J. Clin. Invest.* **2007**, *117* (5), 1219−1222.
(10) Burgess, J. L.; Wyant, W. A.; Abdo Abujamra, B.; Kirsner, R. S.; Jozic, I. Diabetic Wound-Healing Science. *Med.* **2021**, *57* (10), 1072.
(11) Kharaziha, M.; Baidya, A.; Annabi, N. Rational Design of Immunomodulatory Hydrogels for Chronic Wound Healing. *Adv. Mater.* **2021**, *33* (39), No. e2100176.
(12) Blacklow, S. O.; Li, J.; Freedman, B. R.; Zeidi, M.; Chen, C.; Mooney, D. J. Bioinspired mechanically active adhesive dressings to accelerate wound closure. *Sci. Adv.* **2019**, *5* (7), No. eaaw3963.
(13) Zhao, X.; Wu, H.; Guo, B.; Dong, R.; Qiu, Y.; Ma, P. X. Antibacterial anti-oxidant electroactive injectable hydrogel as self-healing wound dressing with hemostasis and adhesiveness for cutaneous wound healing. *Biomaterials* **2017**, *122*, 34−47.
(14) Feig, V. R.; Tran, H.; Lee, M.; Bao, Z. Mechanically tunable conductive interpenetrating network hydrogels that mimic the elastic moduli of biological tissue. *Nat. Commun.* **2018**, *9* (1), 2740.
(15) Song, P.; Qin, H.; Gao, H. L.; Cong, H. P.; Yu, S. H. Self-healing and superstretchable conductors from hierarchical nanowire assemblies. *Nat. Commun.* **2018**, *9* (1), 2786.
(16) Jeon, Y. K.; Jang, Y. H.; Yoo, D. R.; Kim, S. N.; Lee, S. K.; Nam, M. J. Mesenchymal stem cells' interaction with skin: wound-healing effect on fibroblast cells and skin tissue. *Wound Repair Regen.* **2010**, *18* (6), 655−661.
(17) Yan, X.; Fang, W. W.; Xue, J.; Sun, T. C.; Dong, L.; Zha, Z.; Qian, H.; Song, Y. H.; Zhang, M.; Gong, X.; Lu, Y.; He, T. Thermoresponsive *in Situ* Forming Hydrogel with Sol-Gel Irreversibility for Effective Methicillin-Resistant *Staphylococcus aureus* Infected Wound Healing. *ACS Nano* **2019**, *13* (9), 10074−10084.
(18) Li, Y.; Wang, X.; Fu, Y. N.; Wei, Y.; Zhao, L.; Tao, L. Self-Adapting Hydrogel to Improve the Therapeutic Effect in Wound-Healing. *ACS Appl. Mater. Interfaces* **2018**, *10* (31), 26046−26055.
(19) Shah, S. A.; Sohail, M.; Khan, S.; Minhas, M. U.; de Matas, M.; Sikstone, V.; Hussain, Z.; Abbasi, M.; Kousar, M. Biopolymer-based biomaterials for accelerated diabetic wound healing: A critical review. *Int. J. Biol. Macromol.* **2019**, *139*, 975−993.
(20) Zhang, K.; Feng, Q.; Fang, Z.; Gu, L.; Bian, L. Structurally Dynamic Hydrogels for Biomedical Applications: Pursuing a Fine Balance between Macroscopic Stability and Microscopic Dynamics. *Chem. Rev.* **2021**, *121* (18), 11149−11193.
(21) Yates, C.; May, K.; Hale, T.; Allard, B.; Rowlings, N.; Freeman, A.; Harrison, J.; McCann, J.; Wraight, P. Wound chronicity, inpatient care, and chronic kidney disease predispose to MRSA infection in diabetic foot ulcers. *Diabetes care* **2009**, *32* (10), 1907−1909.
(22) Lansdown, A. B.; Mirastschijski, U.; Stubbs, N.; Scanlon, E.; Agren, M. S. Zinc in wound healing: theoretical, experimental, and clinical aspects. *Wound Repair Regen.* **2007**, *15* (1), 2−16.
(23) Alavi, M.; Nokhodchi, A. An overview on antimicrobial and wound healing properties of ZnO nanobiofilms, hydrogels, and bionanocomposites based on cellulose, chitosan, and alginate polymers. *Carbohydr. Polym.* **2020**, *227*, 115349.
(24) Dodero, A.; Scarfi, S.; Pozzolini, M.; Vicini, S.; Alloisio, M.; Castellano, M. Alginate-Based Electrospun Membranes Containing ZnO Nanoparticles as Potential Wound Healing Patches: Biological, Mechanical, and Physicochemical Characterization. *ACS Appl. Mater. Interfaces* **2020**, *12* (3), 3371−3381.
(25) Dong, R.; Zhu, B.; Zhou, Y.; Yan, D.; Zhu, X. "Breathing" vesicles with jellyfish-like on-off switchable fluorescence behavior. *Angew. Chem. Int. Ed.* **2012**, *51* (46), 11633−11637.
(26) Sasidharan, A.; Panchakarla, L. S.; Sadanandan, A. R.; Ashokan, A.; Chandran, P.; Girish, C. M.; Menon, D.; Nair, S. V.; Rao, C. N.; Koyakutty, M. Hemocompatibility and macrophage response of pristine and functionalized graphene. *Small* **2012**, *8* (8), 1251−1263.
(27) Zhou, Q.; Kang, H.; Bielec, M.; Wu, X.; Cheng, Q.; Wei, W.; Dai, H. Influence of different divalent ions cross-linking sodium alginate-polyacrylamide hydrogels on antibacterial properties and wound healing. *Carbohydr. Polym.* **2018**, *197*, 292−304.
(28) Li, D.; Chen, K.; Tang, H.; Hu, S.; Xin, L.; Jing, X.; He, Q.; Wang, S.; Song, J.; Mei, L.; Cannon, R. D.; Ji, P.; Wang, H.; Chen, T. A Logic-Based Diagnostic and Therapeutic Hydrogel with Multistimuli Responsiveness to Orchestrate Diabetic Bone Regeneration. *Adv. Mater.* **2022**, *34* (11), No. e2108430.
(29) Zhao, Z.; Fang, R.; Rong, Q.; Liu, M. Bioinspired nanocomposite hydrogels with highly ordered structures. *Adv. Mater.* **2017**, *29* (45), 1703045.
(30) Brooking, J.; Davis, S. S.; Illum, L. Transport of nanoparticles across the rat nasal mucosa. *J. Drug Targeting* **2001**, *9* (4), 267−279.
(31) Valdiglesias, V.; Costa, C.; Kiliç, G.; Costa, S.; Pásaro, E.; Laffon, B.; Teixeira, J. P. Neuronal cytotoxicity and genotoxicity induced by zinc oxide nanoparticles. *Environ. Int.* **2013**, *55*, 92−100.
(32) Hackenberg, S.; Scherzed, A.; Technau, A.; Kessler, M.; Froelich, K.; Ginzkey, C.; Koehler, C.; Burghartz, M.; Hagen, R.; Kleinsasser, N. Cytotoxic, genotoxic and pro-inflammatory effects of zinc oxide nanoparticles in human nasal mucosa cells in vitro. *Toxicol. In Vitro* **2011**, *25* (3), 657−663.
(33) Saghiri, M. A.; Asatourian, A.; Orangi, J.; Sorenson, C. M.; Sheibani, N. Functional role of inorganic trace elements in angiogenesis-Part II: Cr, Si, Zn, Cu, and S. *Crit Rev Oncol Hematol* **2015**, *96* (1), 143−155.
(34) Kumar, P. T.; Lakshmanan, V. K.; Biswas, R.; Nair, S. V.; Jayakumar, R. Synthesis and biological evaluation of chitin hydrogel/nano ZnO composite bandage as antibacterial wound dressing. *J. Biomed. Nanotechnol.* **2012**, *8* (6), 891−900.
(35) Padmavathy, N.; Vijayaraghavan, R. Enhanced bioactivity of ZnO nanoparticles-an antimicrobial study. *Sci. Technol. Adv. Mater.* **2008**, *9* (3), 035004.
(36) Alavi, M.; Rai, M. Recent progress in nanoformulations of silver nanoparticles with cellulose, chitosan, and alginic acid biopolymers for

https://doi.org/10.1021/acsomega.4c08537
ACS Omega 2024, 9, 51442−51452

antibacterial applications. *Appl. Microbiol. Biotechnol.* **2019**, *103* (21−22), 8669−8676.
(37) Han, G.; Ceilley, R. Chronic wound healing: a review of current management and treatments. *Adv. Ther.* **2017**, *34* (3), 599−610.
(38) Edwards, R.; Harding, K. G. Bacteria and wound healing. *Curr. Opin. Infect. Dis.* **2004**, *17*, 91−96.
(39) Deng, F. H.; He, S. Y.; Cui, S. D.; Shi, Y. Q.; Tan, Y. Y.; Li, Z. J.; et al. A molecular targeted immunotherapeutic strategy for ulcerative colitis via dual-targeting nanoparticles delivering miR-146b to intestinal macrophages. *J. Crohns Colitis.* **2019**, *13*, 482−494.
(40) Liu, C.; Xu, Y.; Lu, Y.; Du, P.; Li, X.; Wang, C.; Guo, P.; Diao, L.; Lu, G. Mesenchymal stromal cells pretreated with proinflammatory cytokines enhance skin wound healing via IL-6-dependent M2 polarization. *Stem Cell Res. Ther.* **2022**, *13* (1), 414.
(41) Shukla, A.; Choudhury, S.; Chaudhary, G.; Singh, V.; Prabhu, S. N.; Pandey, S.; Garg, S. K. (2021). Chitosan and gelatin biopolymer supplemented with mesenchymal stem cells (Velgraft®) enhanced wound healing in goats (Capra hircus): Involvement of VEGF, TGF and CD31. *J. Tissue Viability.* **2021**, *30* (1), 59−66.
(42) Zhang, X.; Chen, G.; Liu, Y.; Sun, L.; Sun, L.; Zhao, Y. Black phosphorus-loaded separable microneedles as responsive oxygen delivery carriers for wound healing. *ACS Nano* **2020**, *14* (5), 5901−5908.
(43) Jiao, Y.; Chen, X.; Niu, Y.; Huang, S.; Wang, J.; Luo, M.; Shi, G.; Huang, J. Wharton's jelly mesenchymal stem cells embedded in PF-127 hydrogel plus sodium ascorbyl phosphate combination promote diabetic wound healing in type 2 diabetic rat. *Stem Cell Res. Ther.* **2021**, *12* (1), 559.
(44) Xiaojie, W.; Banda, J.; Qi, H.; Chang, A. K.; Bwalya, C.; Chao, L.; Li, X. Scarless wound healing: Current insights from the perspectives of TGF-*β*, KGF-1, and KGF-2. *Cytokine Growth Factor Rev.* **2022**, *66*, 26−37.
(45) Lichtman, M. K.; Otero-Vinas, M.; Falanga, V. Transforming growth factor beta (TGF-b) isoforms in wound healing and fibrosis. *Wound Rep. Reg* **2016**, *24* (2), 215−222.
(46) Raina, N.; Haque, S.; Tuli, H. S.; Jain, A.; Slama, P.; Gupta, M. Optimization and Characterization of a Novel Antioxidant Naringenin-Loaded Hydrogel for Encouraging Re-Epithelization in Chronic Diabetic Wounds: A Preclinical Study. *ACS omega* **2023**, *8* (38), 34995−35011.
(47) Bai, Q.; Han, K.; Dong, K.; Zheng, C.; Zhang, Y.; Long, Q.; Lu, T. Potential Applications of Nanomaterials and Technology for Diabetic Wound Healing. *Int. J. Nanomed.* **2020**, *15*, 9717−9743.

https://doi.org/10.1021/acsomega.4c08537
ACS Omega 2024, 9, 51442−51452